University of BRISTOL

DEPARTMENT OF PHYSICS

FINAL YEAR PROJECT

NAME:	Paul Hayes
DEGREE COURSE:	MSci
PROJECT TITLE:	Investigating novel synchronisation effects using bacteria driven microrotors
YEAR OF SUBMISSION:	2019
SUPERVISOR:	Dr. Simon Hanna
NUMBER OF WORDS:	5880

Contents

Declaration

All data presented in this paper has been collected using a python program that I have written myself. My project partner provided insightful discussions regarding the relevant physics in this paper. Guidance has been provided by my supervisor throughout.

Acknowledgements

I am indebted to Dr. Simon Hanna for his patience and guidance throughout this project. Not only has he provided useful insights and suggestions throughout, including his ingenous idea to use an inverted rotor in the shape of a hamster wheel, but has provided me with many amusing hours spent in his office.

I would also like to make a special thanks to my project partner, Connor Gee, who has jointly contributed to the efforts in this project. It has been a pleasure being his partner in labs throughout my four years at University. This project has been a perfect ending to what has been at times a stressful, but mostly hilarious, few years together.

I would also like to extend my gratitude to Robert White, Helena Kingwill and Milo Brent-Carpenter, who have all provided outstanding help throughout this project.

Abstract

A simulation was performed to see if novel in-phase hydrodynamic synchronisation might be observed between neighbouring radially constrained colloids, each driven by a bacteria propelled microrotor. A number of different rotor designs are investigated, with their effect on the rotational frequency and its fluctuation reported. Applying a rotor with the greatest rotational frequency to the total system, a synchronised state mediated by the hydrodynamic interaction was observed. The potential applications for such a system include a targeted drug delivery system, and even the prospect of a more complex macro-machine.

1 INTRODUCTION

Ensembles of interacting active matter display a variety of fascinating collective behaviour. An immediately recognisable example on the macro scale is the cooperative motion of flocks of birds or schools of fish [1, 2]. On the micro scale, self-propelled organisms such as bacteria and spermatozoa exhibit a selection of such collective behaviour. Examples include the spontaneous ordering of bacterial populations into spatiotemporal patterns [3], the formation of bio-films [4], and the emergence of collective synchronous motion in bacterial swarms. This synchronous motion is in part governed by the hydrodynamic interaction [5, 6, 7]. This interaction, mediated by a fluid, is strong and long-ranged. It arises due to interactions between perturbations in the flow of a fluid which surrounds a collection of moving bodies. These bodies act as points of resistance to the fluid flow, coupling to the motion of the other bodies in the system [8]. This coupling underpins the long-ranged nature of the hydrodynamic interaction.

Under appropriate conditions, collections of active matter are able to overcome the restrictions imposed by the second law of thermodynamics, and reach a synchronised state [9]. A pioneering paper from Taylor [10] showed that hydrodynamic synchronisation can occur in low Re systems; in-phase synchrony of the beating tails of neighbouring spermatozoa gave a minimum value for their energy dissipation rate. The exact self-propelling nature of biological micro-swimmers, and of other microscale oscillators, is a crucial component in the emergence of their collective behaviour. Purcells scallop theorem states that, in the low-Re regime, time invariant reciprocal motion cannot produce a net fluid flow [11]. This mandates that under symmetric motion, the position and direction of micro-swimmers in viscous fluids cannot change with time. In addition to this, symmetrical oscillatory motion of the aforementioned spermatozoa tails, or of elastic hair-like organelles called cilia, would deem in-phase synchronisation impossible. Bacteria such as E. Coli overcome this through irreversible processes inside the cell, which take place when converting energy into mechanical motion of flagella to achieve propulsion [12]. The resulting motion breaks time inversion symmetry, and allows for directed movement.

Ryskin and Lenz [13] provided a minimal model of cilia in the form of two rigidly constrained colloids, held at a fixed height above a substrate and forced around circular orbits. Arbitrary motion of arrays with low ciliary densities was found to be insufficient to produce synchronisation. This is a consequence of the invariance of the dynamical equation of motion under the exchange of oscillators; the essential synchronisation condition was not satisfied. Further works have incorporated modifications to this system to achieve synchronisation. Tilting the colloids orbital trajectories in relation to each other was found to be sufficient for their orbital velocities to vary [14]. Additionally, using an arbitrarily varied tangential driving force was enough to bring about synchronisation in a similar system [15, 16].

Active fluids of self-propelled bacteria can be exploited to act as sources of fuel to drive micromachines. The challenge lies in designing a microstructure that gives reproducible directional motions despite the disordered and noisy nature inherent in bacterial suspensions. Initial designs focused on microrobots propelled by bacteria [17, 18, 19, 20, 21, 22], with potential applications in targeted cargo delivery, including drugs. Unfortunately, the motion of these microrobots proved to be random, and the desired directional motion could only be reached by an external feedback signal such as an optical stimuli. More recent studies explored the prospect of bacteria-propelled rotational microrotors. One such study forced bacteria to move along a narrow track that was biochemically attached to a rotor [23, 24]. Although rotational speeds of 2rpm were observed, the motion was highly irregular, with 16 of rotors moving in the opposite direction. It was later demonstrated that due to the nonequilibrium nature of the active baths, spontaneous unidirectional rotation could be induced straightforwardly, with no external stimuli, by ratchets with an asymmetric shape [9, 25]. G. Vizsnyiczai et al. [26] went on to fabricate a unique 3D micro-rotator, which captured individual bacteria so that they could contribute maximally to the applied force. Progress was made here in comparison to previous high noise, low reproducibility microrotor systems. The article concluded with a suggestion that

future studies might explore the effect of hydrodynamic couplings between neighbouring rotors, with potential for the observation of novel synchronisation effects.

The present work will perform a computer simulation of a microrotor driven by a bacterial bath of E.Coli, with the primary aim of investigating these novel synchronisation effects alluded to by G.Vizsnyczai et al.. This simulation follows a similar rotor design to a previous numerical simulation undertaken in [9], which achieved a unidirectional rotation using self-propelled bacteria. Importantly, this current paper will present a number of improvements to the modelling of bacterial dynamics, alongside novel rotor simulation methods and designs. Synchronisation between rotors will be investigated by extending the model previously described by Ryskin and Lenz. This extension follows an adaptation of the model outlined by Niedermayer, Eckhardt and Lenz (NEL) [27], where the colloids, still orbitally constrained, are afforded some degree of radial flexibility. This extra degree of freedom is used as the symmetry breaking parameter needed to observe synchronisation [28].

2 SIMULATION METHOD WITH THEORETICAL DETAILS

2.1 Outline of the Model

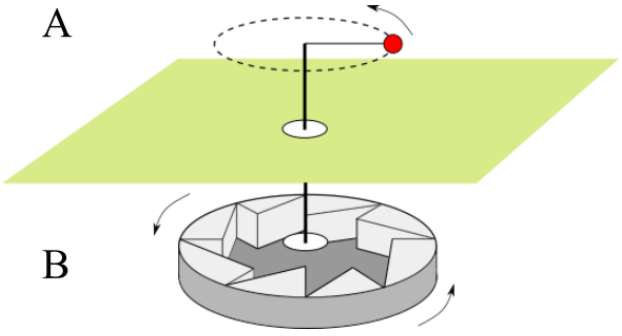

Figure 1: Microrotor (B), contains self-propelling bacteria used to rotate the system. Upper section (A), connected to the microrotor, made up of a bead on a radially constrained orbit. (A) is completely isolated from (B), as outlined by green membrane.

Figure 1 provides a rudimental description of the total system design implemented in this simulation. Bacteria in the lower section (B) are contained within the rotor itself such that they may drive the rotor, as might be expected in a "hamster wheel". The rotor shape was chosen so bacteria may become trapped more readily within the rotor teeth, and contribute maximally where possible to the total torque on the rotor, in a similar vein to that undertaken by G.Vizsnyezai ety al.. Indeed, it was found that when asymmetrical rotors are instead immersed in an external bacterial bath, there is negligible adhesion to the rotor and bacteria will swim away from boundaries after an arbitrary time [9]. Further to this, employing this internal rotor design reduces computational time, due to a reduction in the total number of bacteria needed, and removes any problems that might arise from boundary conditions. The upper half of Figure 1, (A), is completely isolated from the lower section.

This upper section is used to observe if synchronisation between neighbouring rotors is achievable. The model used here is an adaptation of the model devised by NEL, where a bead is constrained in a circular orbit by a spring-like restoring force. The lower section acts as a driving force, similar to the tangential force used in the NEL model.

2.2 Hydrodynamics and the Ermak-McCammon Algorithm

For colloids suspended in a solvent at a low Reynolds number, viscous forces will dominate the inertial. In this regime, the hydrodynamics of colloids are described by the velocity field of their surrounding solvent. Viscous hydrodynamics are governed by Stokes equation for the fluid velocity field, $v_i(\mathbf{r})(i = x, y, z)$,

$$-\eta\partial^2 v_i = -\partial_i p + f_i. \tag{1}$$

Here, $\partial_i = \frac{\partial}{\partial r_i}$, $\partial^2 = \partial_i\partial_j$, with the sum over repeated indices implicit, p is the hydrostatic pressure, η is the viscosity of the fluid and f_i the density of the body force exerted on the fluid[29].

The fluid is modelled as incompressible, which imposes a constraint on the velocity field, where $\delta_j v_j = 0$. Using this with a point force $\mathbf{F}$ located at the origin, EQ.1 then yields the Oseen tensor [30]. This re-

lates the fluid velocity v at a point r, to a point force F,

$$v_i(r) = \frac{1}{8\pi\eta r}(\delta_{ij} + \frac{r_i r_j}{r^2})F_j. \quad (2)$$

with the sum over repeated indices is implicit. Use of the Oseen tensor provides a good approximation to the hydrodynamic interaction, as it has been found to agree well with experimental data [31].

For a system of N Brownian particles, a particle momentum Langevin equation can be written that equates the change in momentum of the particle i to the forces acting on it. Crucially, this relies on the assumption that the distribution of momenta of the particles relaxes to the equilibrium distribution much more rapidly than the particle position distribution. Thus the momentum of the particles may be neglected for the case of low Reynolds number. This leads to the equations of motion for the system as,

$$0 = -\sum_j \mathbf{D}_{ij}^{-1}\mathbf{v}_j + \mathbf{F}_i^{ext} + \mathbf{F}_i^{stoch}(t), \quad (3)$$

where $\mathbf{D}_{ij}^{-1}$ is the configuration-dependent Oseen tensor, v_j is the velocity of the particle j, F_i^{ext} and F_i^{stoch} the external force and stochastic force from brownian motion on particle i, respectively.

Starting with EQ.3, Ermak and McCammon developed [32] an algorithm that describes the particle displacement at successive timesteps Δt. This is written as,

$$r_i = r_i^0 + \sum_j \frac{\delta D_{ij}^0}{\delta r_j}\Delta t + \sum_j \frac{D_{ij}^0 F_j^0}{k_B T}\Delta t + R_i(\Delta t). \quad (4)$$

Here, the superscript "0" indicates the variable needs to be evaluated at the beginning of the time step, r_i is the position of particle i and F_j is the sum of the inter particle and external forces acting on j. The 4th term in the equation, $R_i(\Delta t)$, is the random Brownian displacement which obeys a multivariate Gaussian distribution with mean zero and a covariance of $\langle R_i(\Delta t)R_j(\Delta t)\rangle$, where i and j are particle indices. This equation is how the hydrodynamic interaction is modelled through the simulation.

2.3 Bacteria Driven Microrotor

2.3.1 Bacteria Dynamics

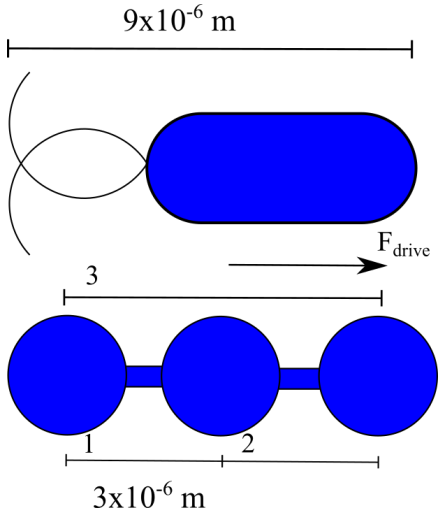

Figure 2: Diagram of a modelled E.Coli bacterium. Bond lengths of 3×10^{-6} are used, with a total length of 3×10^{-6}.

The self-propelling bacteria used as a reference in this simulation are E. Coli. These are rod-shaped organelles with dimensions outlined in FIG.2. The simulation used in [9] straightforwardly used rod-shape organelles in their model. However, this was only achievable based on the assumption that the hydrodynamic effects between the bacteria had a negligible effect on their mean-square displacements. While the exact contribution to the motion of bacteria is widely contested, work by [33] reported that hydrodynamics do indeed play a pivotal role in their dynamics. As such, in order to be thorough in the accuracy of our model, hydrodynamics of the bacteria is implemented using the Ermak-McCammon algorithm in EQ.4. The Ermak-McCammon algorithm is based on an assumption that spheres will be modelled. Therefore, to model a bacterium as a rod, 3 constrained spheres are used. The constraints in this paper are maintained using the LINear Constraint Solver (LINCS) [34]. After an unconstrained update of the bacterial motion mediated by the hydrodynamic interaction, it will constrain the bacteria to its prescribed bond length of 3×10^{-6}.

LINCS is derived as follows: starting from a system of N particles, at positions given by a 3N vec-

tor $\boldsymbol{r}(t)$, an equation of motion derived from Newton's second law is written. The system is then constrained using the principle of least action [35]. Here, the system is constrained by K time-independent constraint equations, added as zero term to the potential $\boldsymbol{V}(\boldsymbol{r})$, multiplied by Lagrange multipliers $\lambda_i(t)$. Using this in the equation of motion, and as the constraint equations are zero and therefore their first and second derivatives, the constraint equation of motion is written as, using $\boldsymbol{T} = \boldsymbol{M}^{-1}\boldsymbol{B}^T(\boldsymbol{B}\boldsymbol{M}^{-1}\boldsymbol{B}^T)^{-1}$,

$$\frac{d^2\boldsymbol{r}}{dt^2} = (\boldsymbol{I} - \boldsymbol{T}\boldsymbol{B})\boldsymbol{M}^{-1}\boldsymbol{f} - \boldsymbol{T}\frac{d\boldsymbol{B}}{dt}\frac{d\boldsymbol{r}}{dt}. \quad (5)$$

Here, $\boldsymbol{M}$ is a $3N$ x $3N$ diagonal matrix containing particle masses, $\boldsymbol{B}$ is a K x $3N$ matrix of the constraint directions, $\boldsymbol{f}$ is a $3N$ force vector, $(\boldsymbol{I} - \boldsymbol{T}\boldsymbol{B})$ is a projection matrix which sets constrained coordinates to zero, $\boldsymbol{B}\boldsymbol{M}^{-1}\boldsymbol{f}$ is a K vector of second derivatives of bond lengths in direction of their bonds and the last term represents centripetal forces caused by rotating bonds [34]. This equation is then discretised using a leap-frog method, which leads to the equation for the constrained positions:

$$\begin{aligned}\boldsymbol{r}_{n+1} &= (\boldsymbol{I} - \boldsymbol{T}_n\boldsymbol{B}_n)r^{unc}_{n+1} + \boldsymbol{T}_n\boldsymbol{d} \\ &= r^{unc}_{n+1} - \boldsymbol{M}^{-1}\boldsymbol{B}_n(\boldsymbol{B}_n\boldsymbol{M}^{-1}\boldsymbol{B}_n^T)^{-1}... \quad (6)\\ &(\boldsymbol{B}_n r^{unc}_{n+1} - \boldsymbol{d}),\end{aligned}$$

where, r^{unc}_{n+1} are positions of the particles after an unconstrained update and $\boldsymbol{d}$ is the length of a bond between two particles. As half the CPU time goes to inverting $\boldsymbol{B}_n\boldsymbol{M}^{-1}\boldsymbol{B}_n^T$ at every time step, a more efficient method of inverting is used. Here, a K x K matrix $\boldsymbol{S}$, the inverse square root of the diagonal of $\boldsymbol{B}_n\boldsymbol{M}^{-1}\boldsymbol{B}_n^T$, is used to give,

$$(\boldsymbol{B}_n\boldsymbol{M}^{-1}\boldsymbol{B}_n^T)^{-1} = \boldsymbol{S}(\boldsymbol{I} - \boldsymbol{A}_n)^{-1}\boldsymbol{S}, \quad (7)$$

where,

$$(\boldsymbol{I} - \boldsymbol{A}_n)^{-1} = \boldsymbol{I} + \boldsymbol{A}_n + \boldsymbol{A}_n^2 + ... \quad (8)$$

Eq.4 may be expanded in a series in this way as the matrix A_n is symmetric and has diagonal values of zero. The different powers of A_n give couplings between bonds equal to the expansion order. Eq.2, along with Eq.3 and Eq.4, are how the algorithm is implemented. [1]

[1] Adapted from previous work by same author, [28]

The Ermak-McCammon algorithm is a long-ranged description of the hydrodynamic effect, breaking down as spheres become too close. Despite this, it gives a sufficient accurate model of the dynamics at smaller separations. To prevent overlap of the spheres causing irreconcilable erroneous values in the Oseen Tensor, a repulsive force is implemented. This force is taken from a previously successful bacterial dynamics simulation undertaken by [36], and is given by,

$$\mathbf{F}(\mathbf{r}) = F_o(\frac{l}{2})^{13}\frac{\mathbf{r}}{|\,\mathbf{r}\,|^{14}}. \quad (9)$$

Here, the prefactor F_o was chosen so that colliding bacteria are at an equilibrium distance of l. The equilibrium distance was chosen to be at least one bond length away, at 3×10^{-6}m.

An E.Coli's propulsion is produced by its flagella, thin helical-like filaments driven by the rotary motors inside the cell. These rotors can bring about motion in two directions: counterclockwise flagella swimming at near-constant linear speeds corresponding to a run, and a clockwise tumble causing unbundling of flagella followed by a random reorientation of the cell [37]. In this simulation, these parameters are fixed such that the bacterium moves at a constant linear speed of vo=20m/s, with a random re-orientation of the cell after a distance of 10 cell lengths. These correspond to physical quantities observed for E.Coli cells.

2.3.2 Microrotor Design

The simulated rotor was designed with the intention that variation of paramters should be straightforward, in order that effects on the rotor rotation would be easily investigated. With this in mind, an equation was derived that describes the exact positions of the whole rotor, based on a simple imput of the number of teeth, N_{teeth}, and the total outer radius of the rotor, r_{outer}. This is defined as,

$$r = r_{outer} - N_{teeth}(\theta + \delta)\%(\frac{2\pi}{factor}). \quad (10)$$

Here, r and θ describe the coordinates of the rotor in polar coordinates, δ is the change in angle of the rotor as it rotates, in radians, and $factor$ is a unit change

depending on the radius of the rotor. The $\%$ symbol is the modulo operator, which finds the remainder after division.

Importantly, this equation may equivalently be used to simplify the complicated nature of the bacterial impacts against the rotor. A coordinate system change is first made, from Cartesian to Polar. Following this, if the radial position of a bacteria is greater than that of the inner radius of a tooth, at the angle of that tooth, then it has collided with that tooth and subsequent impact dynamics may be modelled straightforwardly.

The drag force on the rotor is modelled based on that proposed by [9]. Here, the rotor is assumed to be laying on a liquid-air interface, which results in half the drag force acting at the bottom of the surface being negligible. The rotation rate, Ω, of the rotor may be calculate from the total exerted torque, Γ, from the bacteria, using:

$$\Omega = \frac{3\Gamma}{16\mu R^3}, \tag{11}$$

where R is the radius of the rotor and μ the external buffer viscosity. This has been derived based on a rotational drag coefficient that is twice that of a disk suspended in bulk buffer solution. As the rotor in the paper is near-identical to [9], this equation is sufficient for this simulation.

As reported by [9], any interactions between a bacterium and an object boundary can be well described by a repulsive contact force in a direction along the surface normal. Consequently when a swimming bacterium comes into contact with a wall, it will align and slide parallel to the wall in a direction determined by its incoming angle. For the rotor in section (B) of Figure 1, the bacterium will slide along the surface normal until it preferentially gets trapped in a concave corner, where it will then apply a torque on the rotor. Once a sufficient torque due to multiple bacteria is reached, the rotor will move in a direction determined by its asymmetry.

2.4 Synchronisation between Microrotors

2.4.1 Co-orbiting Constrained Colloids

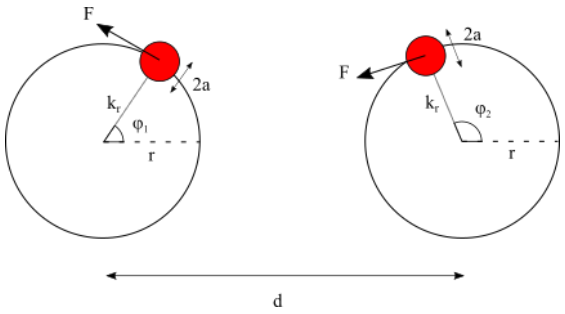

Figure 3: Outline of NEL model used. Red beads of radius a, separated by distance d, move in a circular orbit of radius r, driven by a tangential force, F and constrained via a harmonic restoring force.

The model implemented is a rudimental adaptation of the Ryskin-Lenz model, namely that of NEL. Figure 3 outlines the arrangement of the co-orbiting colloids. These two orbiting beads are the same as those seen in the upper section (A) of Figure 1. Each of the colloids exerts a force on its neighbour, due to the hydrodynamic interaction. If trajectories are fixed radially, any radial component of this force cannot influence the velocity of the neighbouring colloid by altering its orbital radius. Thus, no change in the phase difference can be observed and the velocity is symmetric about its orbit.

However, if a radial flexibility is introduced, determined by the spring constant k_r, changes in the orbital radius brought on by the hydrodynamic interaction may asymmetrical change the velocity of the colloid. Over the course of several rotations, under the right conditions, the two colloids will synchronise. This synchronisation is a consequence of the drag force parallel motion being half as large compared to colloids moving in-line [27].

3 RESULTS

The following sections begin with a number of results for an isolated microrotor driven by bacteria. This is used as a callibration to find the ideal system that can produce the highest rotational frequencies with the smoothest output. Following this, both sections

are combined to observe if neighbouring rotors may synchronise.

If not otherwise stated, the default parameters used throughout are: $timestep$ = 1×10^{-4}s, r_{outer}= 1×10^{-5}m, N_{teeth}=14, $Bacterial\ concentration$ = 1×10^{9}bacteria/mL, $viscosity$ = 0.001 Pa.s and T=300K.

3.1 Bacteria driven Microrotor

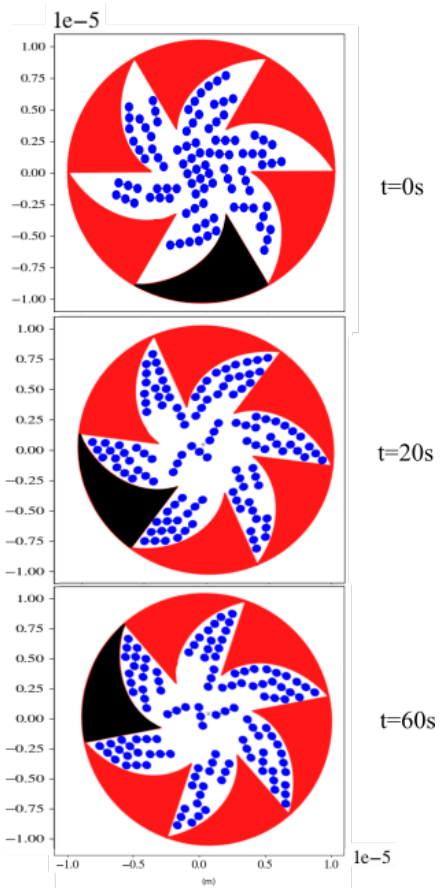

Figure 4: 2D slice of the microrotor position as a function of time. Initial time, t=0, chosen after a transient period to allow bacteria to spread through rotor. Three connected spheres indicate a bacterium. The black section has been included to highlight rotation.

Figure 4 gives a 2D slice of the simulated microrotor at varying times. As demonstrated by the black section, after the bacteria, seen in blue, become entrapped in the corners and exerting a torque, a net rotation is observed.

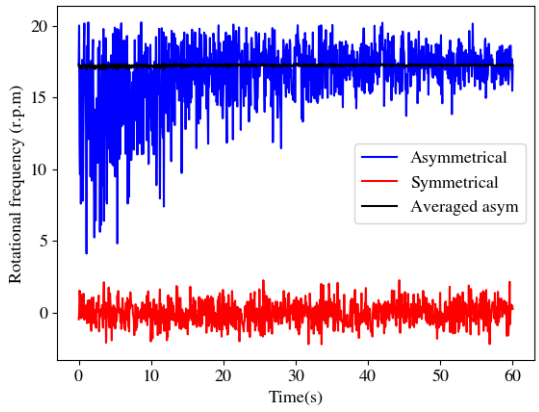

Figure 5: Rotation rate in r.p.m. of a rotor as a function of time. Comparisons are made of an asymmetrical to symmetrical shape. Mean value of asymetrical rotation rate, seen by black line, is 17.4 $\pm$ 0.4 r.p.m.., from repeated simulations

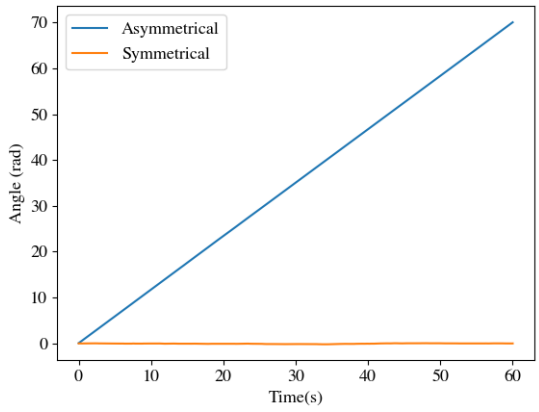

Figure 6: Commulative change in angle of Asymmetrical (blue) and Symmetrical (orange) rotor design. Asymmetrical rotor shows a smooth, linear increase with time, whereas symmetrical rotor shows no net change.

Figure 5 reveals the dependence on a net unidirectional rotational frequency with the design of a rotor. Clearly, there is no net rotation for a symmetrical rotor, with rotational frequencies fluctuating about a value of 0 $\pm$ 1.2 r.p.m.. The incorporation of an asymmetrical component alone gives a net average rotation rate of 17.4 $\pm$ 0.4 r.p.m.. The fluctua-

tions seen in the rotational frequency may in part be attributed to the timestep used, wherein a disproportionally low number of bacteria may be seen to collide with a wall in this time. This would create spikes in the rotational frequency for that timestep, which is indeed observed. The sharp spikes seen may also be explained as bacteria colliding with the long edge of the rotor, generating a torque in the opposing direction to the rotation. Interestingly, for the asymmetrical design, the fluctuations about its mean rotation rate decreases with time, with variations of 66% of its mean rotational frequency of 18.6 r.p.m. decreasing to 11% after 60s. Additionally, there appears to be a limit in the achievable rotational frequency, at around 20 r.p.m..

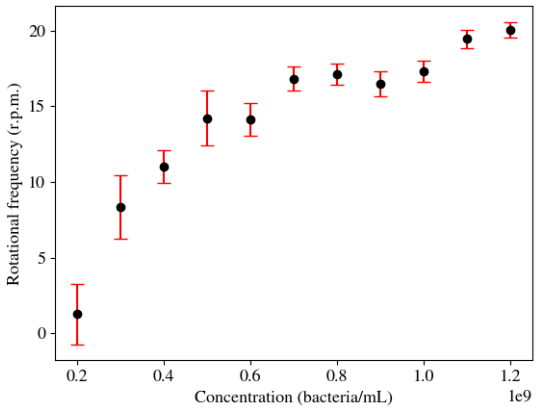

Figure 7: Rotational frequency with varying bacteria concentrations using an asymmetrical rotor. An initial increase in rotational frequency is observed, with an expected limit found at around 17.5 r.p.m.. Error bars seen are from repeated simulations. The decrease in error at high concentrations is noted.

Despite the asymmetrical rotor having fluctuations about its mean rotational frequency, its cumulative change in angle shows a much smoother output. This is shown in Figure 6. This may be simply explained due to the relatively small change in angle of the rotor at each timestep, at an average of 0.00019 radians per timestep of 1×10^{-4}, in comparison to the greater fluctuations in the rotational frequency due to a change in the number of bactera colliding in the timestep. Most importantly, however, the asymmetrical rotor's cumulative angle over time is stable and unidirectional, in contrast to the stable yet nondirectional symmetrical rotor.

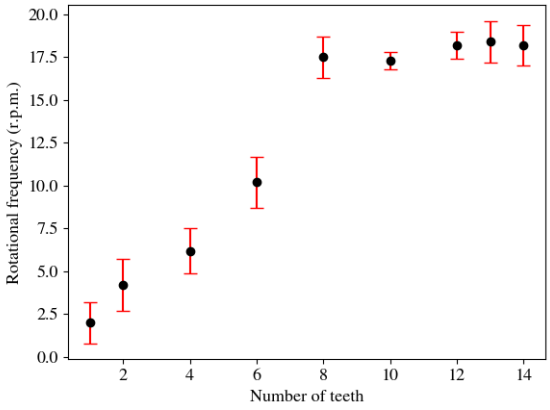

Figure 8: Rotational frequency as a function of the number of teeth in an aymmetrical rotor. An initial increase in rotational frequency is seen, but appears to reach a maximum at 17.6 r.p.m..

Figure 7 illustrates how varying bacterial concentration affects rotational frequency of the rotor. It might be expected that if more bacteria are able to contribute to the torque, the rotational rate will be greater. This is clearly apparent for concentrations up to 0.7×10^{9} bacteria/mL, yet breaks down at higher concentrations where the rotational frequency approaches an asymptote and fluctuates around 17.5 r.p.m..

Figure 8 reveals a similar trend to the concentration, with an unsurprising initial increase in rotational frequency with the addition of further teeth, yet leveling off at a similar rotional frequency of around 17.6 r.p.m..

3.2 Synchronisation Between Microrotors

The bacteria driven microrotor may be seen as a force generator for the tangential force applied in the model applied by NEL. Simulations were run to investigate if the magnitude of the force from bacteria alone is sufficient to induce synchronisation in this model. Using the previous section as a form of calibration, this system produced the range of forces seen in Figure 9. The effect of the previous calibrations are performed to reduce the standard deviation of this gaussian and increase its mean value. Therefore, it was found that using the ideal parameters as described in previous plots, gives a mean of 2.7×10^{-11}N and standard deviation 1.6×10^{-11}N.

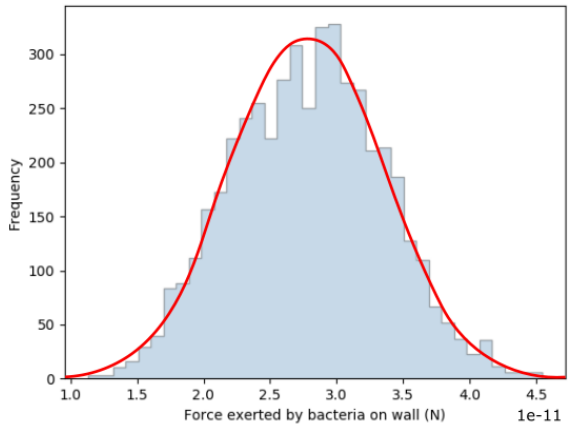

Figure 9: Histogram of total force exerted by bacteria on a rotor over a number of timesteps. A gaussian with mean 2.7×10^{-11}N and standard deviation 1.6×10^{-11}N is fitted to the data.

The degree of freedom, a spring-like restoring force, is applied radially to the rotating colloid and its effect on inducing synchronisation is explored. This is seen in Figure 8. The plot confirms the NEL findings, that a system with less flexibility takes longer to synchronise, as seen in for the k=100×10^{7}N/m case.

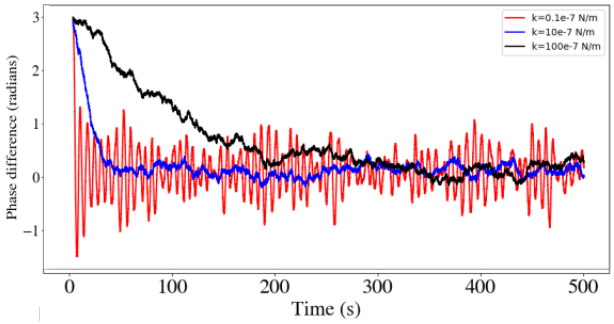

Figure 10: Phase difference between co-orbiting constrained colloids for varying degrees of radial stiffness. Curves appear to oscillate about a difference in phase of zero after a given time. Greater radial stiffness shows an increased time for zero phase difference to be observed.

Clearly, Figure 10 shows this system is able to reach a synchronised state after a given amount of time. The degree of synchronisation, however, will be found by the following method. Previous work has successfully applied an autocorrelation function which relates the difference in phases of the colloids at steady state, with the strength of the synchronised state [38]. This autocorrelation function is a measure which describes how consistent a difference in phase between oscillators remains with time. The autocorrelation, $A(dt)$, with time is defined as:

$$A(dt) = \frac{\langle q(t) \times q(t+dt) \rangle}{COV}. \tag{12}$$

Here, $q(t)$ is the difference in phase between two colloids at a projected time in the future, and $q(t+dt)$ is this difference in phase at a further dt. COV is the covariance of the difference in phase, found from the numerator of the autocorrelation function at a time dt=0. The covariance is a normalising factor in the autocorrelation function. Values of 1 will therefore indicate perfect positive correlation, -1 perfect negative and 0 no correlation.

EQ.12 can be used to give curves of the autocorrelation of the phase difference between oscillators with respect to dt. These curves are expected to follow an exponential decay with a given relaxation time, matching that of a damped harmonic oscillator. This is expected to follow [39]:

$$S(dt) = Ae^{-\beta dt} \tag{13}$$

where A is fixed to 1 by normalisation and β^{-1} is the relaxation time of the system, meaning that β is the synchronisation strength of the system in units of inverse time. The subsequent curves in this section are made by applying a non-linear least squares fit of the autocorrelation function, using EQ.13, to obtain values of the synchronisation strength for different system parameters.

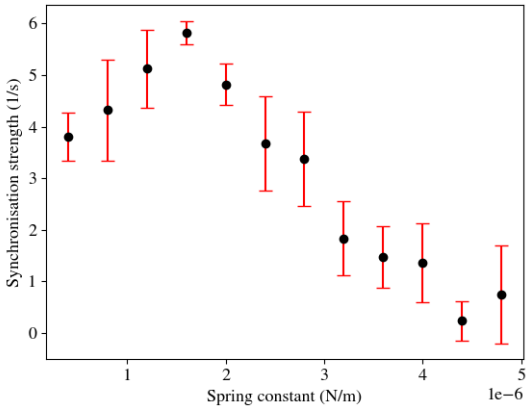

Figure 11: Synchronisation strength as a function of the spring constant, a peak is seen at 1.8×10^{-6}.

NEL predict that the synchronisation strength should decrease as the system becomes more rigid, as a consequence of the reduction in the flexibility of this degree of freedom. This is evident in Figure 9, beyond values of the spring constant, k, of $1\times10^{-6}Nm^{-1}$. However, there appears to be an unpredicted peak at this value, where at lower k values the synchronisation strength decreases.

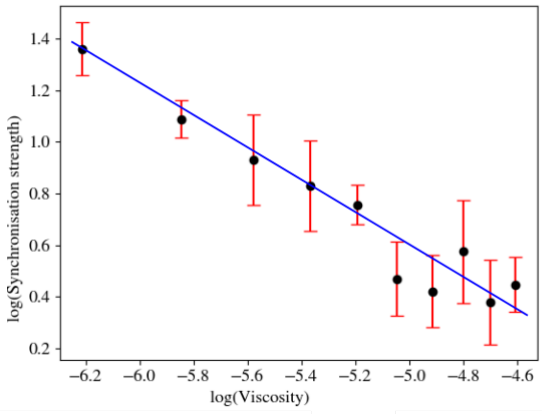

Figure 12: Log-log plot of viscosity as a function of synchronisation strength. A linear gradient of -0.66 $\pm$ 0.23 is observed, confirming the expected inverse relation. Error bars seen are standard error, calculated from repeated simulations.

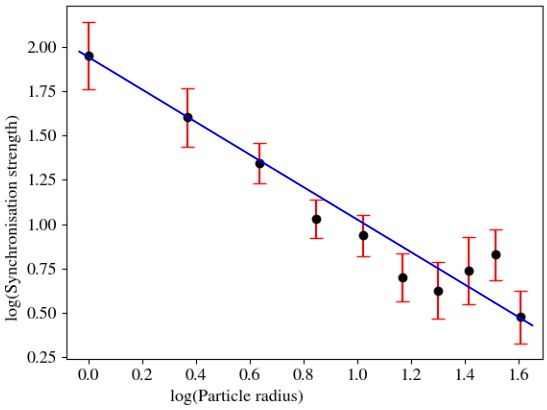

Figure 13: Log-log plot of particle radius as a function of synchronisation strength. A linear gradient of -1.02 $\pm$ 0.13 is observed, confirming the expected inverse relation. Error bars seen are standard error, calculated from repeated simulations.

Figures 12 and 13 are log-log plots of the relationship between the viscosity of the solvent and the colloid's radius, respectively, with the measured synchronisation strength. Both plots show a linear relationship, with a gradient of -0.66 $\pm$ 0.23 in Figure 12 and -1.02 $\pm$ 0.13 in Figure 13.

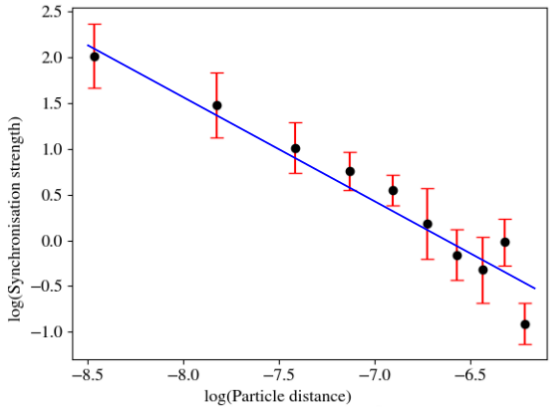

Figure 14: Log-log plot of particle separation as a function of synchronisation strength. A linear gradient of -1.25 $\pm$ 0.31 is observed, confirming the expected inverse relation. Error bars seen are standard error, calculated from repeated simulations.

Figure 14 shows the dependence on the separation between rotors and their synchronisation strength. Clearly, as their separation increases there is a inverse relation with the strength of synchronisation.

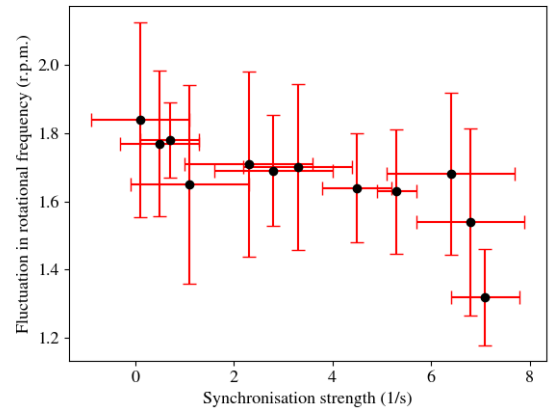

Figure 15: Rotational frequency fluctuation and its relation to synchronisation strength of the system. Errors seen are from repeated simulations.

Figure 15 shows an investigation into whether there is any dependence on the fluctuations in rotational frequency of the system and the synchronisation strength. It is hypothesised that there might be a decrease in the fluctuation at greater synchronised states. However, no trend is discernable as the overlap of the errors mean there are no significant differences between fluctuations in rotational frequency.

4 DISCUSSION

4.1 Bacteria driven Microrotor

Previous experimentation has observed the speed of freely swimming E.Coli to be $20\mu ms^{-1}$ [26]. With the bacteria moving at this speed, therefore, there will be a limit on the maximum achievable rotational frequency of the rotor, as the bacteria will not be able to keep up with the rotation. The measured average rotational frequency of an asymmetrical microrotor of 17.4 $\pm$ 0.4 r.p.m., corresponds to a linear speed of the rotor's outer edge of 18.2 $\pm$ 0.5μms^{-1} in this simulation, using a rotor radius of 1×10^{-5}m. The discrepancy between the linear speed of the rotor and the bacteria's free swimming speed could simply be a consequence of the bulk drag force of the rotor, modelled by EQ.4. Whereas G. Vizsnyical et al. [26] found higher rotational frequencies of 20 r.p.m. for a rotor of equal size, they reported a rotational drag of 9.4 $\pm$ 0.2 pNμmsrad^{-1} for their rotor. From EQ.4, the rotor used in this simulation will have a rotational drag of 10.6 pNμmsrad^{-1}. If instead of this, the rotational drag from G. Vizsnyical et al. is incorporated into the simulation, the rotational frequencies simulated increase to an average of 20.1 r.p.m.. Clearly, therefore, the rotational drag on our system is the dominant limiting factor in producing higher rotational frequencies. Thus, a rotor design that mimicks that of G. Vizsnyical et al. would provide higher rotational frequencies than the cylindrical shaped rotor in this simulation.

Over time, it was observed that the rotational frequencies for a rotor became less noisy, with variations of 66% about its mean rotational frequency of 17.4 r.p.m. decreasing to 11% after 60s. Initially, the bacteria are positioned evenly throughout the inside of the rotor. As the simulation progresses, the bacteria eventually are seen to clump together, with a majority of the bacteria positioned within the teeth of the rotor. This simulated behaviour seems to mimic the cooperative action of bacteria, where in concen-

trated suspensions, bacteria become locally packed and ordered at concave corners. This behaviour is due to the interactions with the wall and intercellular interactions between bacteria [9]. The cooperative behaviour of the bacteria around the teeth is therefore a compelling explanation for the reduction in the rotor's angular frequency noise, as it will reduce the stochastic nature of the impacts. Fluctuations in the angular frequency beyond this might be due to the run and tumble dynamics of a bacteria, where after some time they might become dislodged from the confinement due to their local packing around the teeth.

Increasing the number of teeth in a rotor initially increases the measured rotational frequency, yet there is a point where no further increases are observed. Obviously, the initial increase can be attributed to an increase in the total applied torque in the direction of its asymmetry. However, at higher teeth numbers, the subsequent the size of the gap between teeth that a bacteria can occupy reaches the size of an individual E.Coli bacteria. At this point there can be no further increase to the rotational frequency as no more bacteria can fit inside a tooth and contribute to the torque. Similarly, the increasing the concentration of bacteria will initially increase rotational frequency and reduce its fluctuation, however once the bacteria reach a maximum packing, there cannot be any further benefit.

4.2 Synchronisation Between Microrotors

Measurements of the phase difference between two co-orbiting colloids, driven by bacteria powered microrotor, showed that a degree of freedom in its radial flexibility was sufficient to produce synchronisation. Clearly, in Figure 10, the amount of time for the phase difference to reach a synchronised state depends strongly on its radial stiffness. In agreement with Ryskin and Lenz [13], a more rigid system, k=100×10^{-7}N/m, reaches synchrony in a greater time than for a more weakly bound system, k=10×10^{-7}N/m in the form of a Niedermayer et al. type model. Further to this, at a spring constant of k=100×0.1^{-7}N/m, the system reaches synchrony but there is clear increase in the oscillation about its synchronised state. This is likely due to relatively high degree of flexibility in comparison to the tangential force applied. In this scenario, the tangential force would bring the colloid further outside its orbital radius.

In addition to the time to reach a synchronised state, an investigation into the strength of this state was made with respect to the radial stiffness used. For an increase in the radial flexibility, NEL predict that the system should have more freedom to synchronise and therefore do so faster and with greater stength. Figure 11 agrees with this expectation, with an decrease in synchronisation strength for a more rigid system at k>1.8×10^{-6}N/m. Yet, at lower values of the spring constant, corresponding to a more weakly bound system, there is an unpredicted decrease in the synchronisation strength. This can be explained in a similar vein to the previously discussed phase difference graph. The tangential force at this radial stiffness might dominate the motion of the colloid, meaning the system is more weakly bound and perhaps less strongly synchronised. If this is not the case, it might be a consequence of the fitting function to the autocorrelation function breaking down as it approachs a system that it too strongly synchronised. This might occur if the autocorrelation function does not decay, but stays at an infinitely synchronised system. The fitting function used will not be able to describe this behaviour accurately.

Simulating the stength of the hydrodynamic interaction between colloids is directely related to the magnitude of Oseen tensor. This magnitude is inversely related to the drag coefficient of a sphere, $(6\pi\eta a)$ [38]. This explains the trends seen in Figures 12 and 13. Here, the straight line in the log-log plots, with gradient of -0.66 $\pm$ 0.23 and -1.02 $\pm$ 0.13 respectively, confirm this inverse relation. However, the gradient Figure 12 does not agree with expected gradient of -1 for an inversely proportional relation. This might be due to the errors seen in the system. However, the error observed for the gradient does not fully account for this descrepancy. This suggests that the model might have broken down at certain viscosities, giving erronous results. The strength of hydrodynamic synchronisation between colloids is directly related to the strength of the hydrodynamic interaction between them. Therefore lessening of the hydrodynamic interaction from the Oseen tensor would ex-

pect to see a reduction in the synchronisation strength measured.

The separation of colloids is expected to show an inverse relation with the strength of synchronisation. Figure 14 shows a gradient of -1.25 $\pm$ 0.31., however, it is noted that the linear fit between these data might not sufficiently describe the trend. The Rotne-Prager tensor gives the second order term in the power series that describes the hydrodynamic interaction. This is not present in the Oseen Tensor [32]. This provides a more accurate description of the hydrodynamic interaction, but breaks down at smaller distances. As separation of the colloids increases, the Oseen Tensor may not be sufficient in modelling the interaction. Therefore, this might explain the unexpected divergence from a non-linear graph seen in Figure 14.

A very interesting point of analysis is the investigation into whether the strength of synchronisation between neighbouring rotors can impact the fluctuations in the rotational frequency of the system. Figure 15 presents a number of systems of varying synchronisation strengths along with its observed fluctuation in rotational frequency. No clear trend can be interpreted, due to magnitude in the errors inherent in this simulation. It is noted, however, that there does seem to be a decrease in fluctuation. A number of theories can be made for the expected trend of this curve. The fluctuations in rotational frequency for an isolated microrotor was found to be 0.4 r.p.m., or 0.04 rad s^{-1}. Inspecting Figure 8, the maximum fluctuations in phase difference for the synchronised state at k=10×10^{-7} is 0.02 rad s^{-1}. Clearly, with the addition of synchronisation achieved upper section of the system, this suggests there has been a reduction in the observed fluctuation in angle of the rotor. If future studies achieve a system with lower errors, this effect might be more discernable. Of course, there should be a limit to any reduction in fluctuation. This is due to the inherently noisy nature of self-propelled bacteria. However, this limit has clearly not been reached in this simulation.

4.3 Further Considerations

Simulations of this nature are vital to the fabrication of microrotors in this field. Investigations into a rotor design that produces the greatest unidirectional rotational frequency with the smallest degree of fluctuations can be performed with high efficiency, in contrast to time consuming physical fabrications.

The justification of using E. Coli is that they are efficient swimmers of the right size, and as the majority of E. Coli cells are not harmful to the human body, drug delivery is just one of the compelling applications of this system. Despite this, a potential improved system might use one of the fastest swimming bacteria known, *Thiovulum majus* [40]. Not only do these bacteria move at six times that of E. Coli, but through their collective behaviour they may arrange themselves into a stable hexagonal lattice. This might be a very interesting application to the field of bacteria powered microrotors as this stable configuration might reduce the current observed noise associated such systems. Importantly, however, this might overcome the limit in the rotational frequencies due to the free swimming speed of E. Coli previously discussed.

A fundamental flaw with this microrotor design is that the bacteria inside it will die over time, and in contrast to other rotors where bacteria are on its exterior, this will give it a shorter lifetime. However, the results obtained in this paper remain of high use, as a simple adaptation to the rotor design such as the trapping mechanism used by G. Vizsnyical et al. may be used. These two models can be seen as near identical, the 'hamster wheel' design was simply chosen to increase computational efficiency. Yet, the finite time of these microrotors is inherent in any bacteria powered system, but this is the price to pay for avoiding the need for an external power source.

5 CONCLUSIONS

A simulation was performed to see if novel in-phase hydrodynamic synchronisation might be observed between neighbouring radially constrained colloids, each driven by a bacteria propelled microrotor. Varying designs of microrotors were tested to arrive at a rotor that gave the greatest smooth, undirectional rotation. This design was then applied to a model similar to that by NEL, and it was ultimately found that in-phase synchronisation could indeed be observed for such a system.

A number of parameters in the system were investigated for their effect on the strength of this hydrody-

namic synchronisation. Expected relations between these parameters were mostly successfully produced. Finally, an investigation into the feedback between the bacteria powered microrotor and the NEL model was performed, looking at the relation between the strength of the synchronised state with the fluctuations in the rotational frequency of the system. However, due to errors inherent in the system, no discernible trend could be seen.

The system devised in this paper shows promising application to a self organised micro-fluidic device, whereby an array of such systems might move in synchrony and be used to direct cargo smoothly without need for an external power source. Ambitiously, a large number of synchronised bacteria powered microrotors might one day be exploited as part of a self-contained macro-machine.

References

[1] Christos C Ioannou, Vishwesha Guttal, and Iain D Couzin. Predatory fish select for coordinated collective motion in virtual prey. *Science*, 337(6099):1212–1215, 2012.

[2] Michele Ballerini, Nicola Cabibbo, Raphael Candelier, Andrea Cavagna, Evaristo Cisbani, Irene Giardina, Vivien Lecomte, Alberto Orlandi, Giorgio Parisi, Andrea Procaccini, et al. Interaction ruling animal collective behavior depends on topological rather than metric distance: Evidence from a field study. *Proceedings of the National Academy of Sciences*, 105(4):1232–1237, 2008.

[3] Christopher Dombrowski, Luis Cisneros, Sunita Chatkaew, Raymond E Goldstein, and John O Kessler. Self-concentration and large-scale coherence in bacterial dynamics. *Physical Review Letters*, 93(9):098103, 2004.

[4] Luanne Hall-Stoodley, J William Costerton, and Paul Stoodley. Bacterial biofilms: from the natural environment to infectious diseases. *Nature Reviews Microbiology*, 2(2):95, 2004.

[5] Luanne Hall-Stoodley, J William Costerton, and Paul Stoodley. Bacterial biofilms: from the natural environment to infectious diseases. *Nature Reviews Microbiology*, 2(2):95, 2004.

[6] Qian Liao, Ganesh Subramanian, Matthew P DeLisa, Donald L Koch, and Mingming Wu. Pair velocity correlations among swimming escherichia coli bacteria are determined by force-quadrupole hydrodynamic interactions. *Physics of Fluids*, 19(6):061701, 2007.

[7] Eric Lauga and Thomas R Powers. The hydrodynamics of swimming microorganisms. *Reports on Progress in Physics*, 72(9):096601, aug 2009.

[8] Hiromi Yamakawa. *Modern theory of polymer solutions*. Harper & Row, 1971.

[9] R Di Leonardo, L Angelani, D DellArciprete, Giancarlo Ruocco, V Iebba, S Schippa, MP Conte, F Mecarini, F De Angelis, and E Di Fabrizio. Bacterial ratchet motors. *Proceedings of the National Academy of Sciences*, 107(21):9541–9545, 2010.

[10] Geoffrey Ingram Taylor. Analysis of the swimming of microscopic organisms. *Proceedings of the Royal Society of London. Series A. Mathematical and Physical Sciences*, 209(1099):447–461, 1951.

[11] Edward M Purcell. Life at low reynolds number. *American Journal of Physics*, 45(1):3–11, 1977.

[12] Luca Angelani, Roberto Di Leonardo, and Giancarlo Ruocco. Self-starting micromotors in a bacterial bath. *Physical Review Letters*, 102(4):048104, 2009.

[13] Peter Lenz and Andrey Ryskin. Collective effects in ciliar arrays. *Physical Biology*, 3(4):285, 2006.

[14] Andrej Vilfan and Frank Jülicher. Hydrodynamic flow patterns and synchronization of beating cilia. *Physical Review Letters*, 96(5):058102, 2006.

[15] Nariya Uchida and Ramin Golestanian. Synchronization and collective dynamics in a carpet of microfluidic rotors. *Physical Review Letters*, 104(17):178103, 2010.

[16] Nariya Uchida, Ramin Golestanian, and Rachel R Bennett. Synchronization and collective dynamics of flagella and cilia as hydrodynamically coupled oscillators. *Journal of the Physical Society of Japan*, 86(10):101007, 2017.

[17] Bahareh Behkam and Metin Sitti. Bacterial flagella-based propulsion and on/off motion control of microscale objects. *Applied Physics Letters*, 90(2):023902, 2007.

[18] Edward Steager, Chang-Beom Kim, Jigarkumar Patel, Socheth Bith, Chandan Naik, Lindsay Reber, and Min Jun Kim. Control of microfabricated structures powered by flagellated bacteria using phototaxis. *Applied Physics Letters*, 90(26):263901, 2007.

[19] Sung Jun Park, Hyeoni Bae, Joonhwuy Kim, Byungjik Lim, Jongoh Park, and Sukho Park. Motility enhancement of bacteria actuated microstructures using selective bacteria adhesion. *Lab Chip*, 10:1706–1711, 2010.

[20] Edward B Steager, Mahmut Selman Sakar, Dal Hyung Kim, Vijay Kumar, George J Pappas, and Min Jun Kim. Electrokinetic and optical control of bacterial microrobots. *Journal of Micromechanics and Microengineering*, 21(3):035001, feb 2011.

[21] Rika Wright Carlsen, Matthew R. Edwards, Jiang Zhuang, Cecile Pacoret, and Metin Sitti. Magnetic steering control of multi-cellular bio-hybrid microswimmers. *Lab Chip*, 14:3850–3859, 2014.

[22] Jaideep Katuri, Xing Ma, Morgan M. Stanton, and Samuel Snchez. Designing micro- and nanoswimmers for specific applications. *Accounts of Chemical Research*, 50(1):2–11, 2017. PMID: 27809479.

[23] Yuichi Hiratsuka, Makoto Miyata, and Taro Q.P. Uyeda. Living microtransporter by uni-directional gliding of mycoplasma along microtracks. *Biochemical and Biophysical Research Communications*, 331(1):318 – 324, 2005.

[24] Yuichi Hiratsuka, Makoto Miyata, Tetsuya Tada, and Taro Q. P. Uyeda. A microrotary motor powered by bacteria. *Proceedings of the National Academy of Sciences*, 103(37):13618–13623, 2006.

[25] Andrey Sokolov, Mario M. Apodaca, Bartosz A. Grzybowski, and Igor S. Aranson. Swimming bacteria power microscopic gears. *Proceedings of the National Academy of Sciences*, 107(3):969–974, 2010.

[26] Gaszton Vizsnyiczai, Giacomo Frangipane, Claudio Maggi, Filippo Saglimbeni, Silvio Bianchi, and Roberto Di Leonardo. Light controlled 3d micromotors powered by bacteria. *Nature Communications*, 8:15974, June 2017.

[27] Thomas Niedermayer, Bruno Eckhardt, and Peter Lenz. Synchronization, phase locking, and metachronal wave formation in ciliary chains. *Chaos: An Interdisciplinary Journal of Nonlinear Science*, 18(3):037128, 2008.

[28] Paul Hayes. Computational modelling of bacteria driven microrotors. 2018.

[29] Ramin Golestanian, Julia M. Yeomans, and Nariya Uchida. Hydrodynamic synchronization at low reynolds number. *Soft Matter*, 7:3074–3082, 2011.

[30] J. Happel and H. Brenner. Low reynolds number hydrodynamics. 1 1983.

[31] K. Zahn, J. M. Méndez-Alcaraz, and G. Maret. Hydrodynamic interactions may enhance the self-diffusion of colloidal particles. *Physical Review Letters*, 79:175–178, Jul 1997.

[32] Donald L. Ermak and J. A. McCammon. Brownian dynamics with hydrodynamic interactions. *The Journal of Chemical Physics*, 69(4):1352–1360, 1978.

[33] Aparna Baskaran and M. Cristina Marchetti. Statistical mechanics and hydrodynamics of bacterial suspensions. *Proceedings of the National Academy of Sciences*, 106(37):15567–15572, 2009.

[34] Berk Hess, Henk Bekker, Herman J. C. Berendsen, and Johannes G. E. M. Fraaije. Lincs: A linear constraint solver for molecular simulations. *Journal of Computational Chemistry*, 18(12):1463–1472.

[35] Makoto Yoneya, H. J. C. Berendsen, and Kootaro Hirasawa. A non-iterative matrix method for constraint molecular dynamics simulations. *Molecular Simulation*, 13(6):395–405, 1994.

[36] L. Angelani and R. Di Leonardo. Numerical modeling of bacteria propelled micromotors. *Computer Physics Communications*, 182(9):1970 – 1973, 2011. Computer Physics Communications Special Edition for Conference on Computational Physics Trondheim, Norway, June 23-26, 2010.

[37] Howard C.Berg. *E.Coli in Motion*. 2004.

[38] Jurij Kotar, Luke Debono, Nicolas Bruot, Stuart Box, David Phillips, Stephen Simpson, Simon Hanna, and Pietro Cicuta. Optimal hydrodynamic synchronization of colloidal rotors. *Phys. Rev. Lett.*, 111:228103, Nov 2013.

[39] Milo Brent-Carpenter. Modelling hydrodynamic synchronisation in nearest and next-nearest neighbour pairs, 2018.

[40] Alexander P Petroff, Xiao-Lun Wu, and Albert Libchaber. Fast-moving bacteria self-organize into active two-dimensional crystals of rotating cells. *Physical Review Letters*, 114(15):158102, 2015.

Appendix

Project Report presented as part of, and in accordance with, the requirements for the Final Degree of MSci at the University of Bristol, Faculty of Science.

Author Paul Hayes

Title Investigating novel synchronisation effects using bacteria driven microrotors.

Date of submission 30/04/2019

Signed: Paul Hayes

Full name: Paul Hayes

Date: 30/4/2019